Published in "Biochimica et Biophysica Acta (BBA) - Molecular Cell Research 1833(7): 1680–1691, 2013" which should be cited to refer to this work.

Mechanism of capsaicin receptor TRPV1-mediated toxicity in pain-sensing neurons focusing on the effects of Na^+/Ca^{2+} fluxes and the Ca^{2+}-binding protein calretinin

László Pecze, Walter Blum, Beat Schwaller *

Unit of Anatomy, Department of Medicine, University of Fribourg, Route Albert-Gockel 1, CH-1700 Fribourg, Switzerland

Transient receptor potential vanilloid subtype 1 (TRPV1) receptor is a pain-sensing, ligand-gated, non-selective cation channel expressed in peripheral sensory neurons. Prolonged activation of TRPV1 by capsaicin leads to cell swelling and formation of membrane blebs in rat dorsal root ganglion (DRG) neurons. Similar results were obtained in NIH3T3 fibroblast cells stably expressing TRPV1. Here, we assessed the contribution of Ca^{2+} and Na^+ ions to TRPV1-mediated changes. Cell swelling was caused by a substantial influx of extracellular Na^+ via TRPV1 channels, causing concomitant transport of water. In the absence of extracellular Na^+, the membrane blebbing was completely inhibited, but Ca^{2+} influx did not change under these conditions. Na^+ influx was modulated by the intracellular Ca^{2+} concentration ($[Ca^{2+}]_i$). Elevation of $[Ca^{2+}]_i$ by ionomycin sensitized/activated TRPV1 channels causing cell swelling in TRPV1-positive cells. In the absence of extracellular Ca^{2+}, capsaicin caused only little increase in $[Ca^{2+}]_i$ indicating that the increase in $[Ca^{2+}]_i$ observed after capsaicin application is derived essentially from extracellular Ca^{2+} and not from internal Ca^{2+} stores. In the absence of extracellular Ca^{2+} also the process of cell swelling was considerably slower. Calretinin is a Ca^{2+} buffer protein, which is expressed in a subset of TRPV1-positive neurons. Calretinin decreased the amplitude, but slowed down the decay of Ca^{2+} signals evoked by ionomycin. Cells co-expressing TRPV1 and calretinin were less sensitive to TRPV1-mediated, capsaicin-induced volume increases. In TRPV1-expressing NIH3T3 cells, calretinin decreased the capsaicin-induced Ca^{2+} and Na^+ influx. Swelling and formation of membrane blebs resulted in impaired plasma membrane integrity finally leading to cell death. Our results hint towards a mechanistic explanation for the apoptosis-independent capsaicin-evoked neuronal loss and additionally reveal a protective effect of calretinin; we propose that the Ca^{2+}-buffering capacity of calretinin reduces the susceptibility of calretinin-expressing DRG neurons against cell swelling/death caused by overstimulation of TRPV1 channels. This article is part of a Special Issue entitled:12th European Symposium on Calcium.

1. Introduction

Transient receptor potential vanilloid type 1 (TRPV1) is one of the main pain-sensing receptors in sensory neurons [1,2]. TRPV1 forms a homo-tetramer with six trans-membrane segments per monomer; the N- and C-termini are intracellular. The cation pore is formed by P-loops of the four monomers and the P loop is the region between trans-membrane domains 5 and 6 [3]. When opened, both Na^+ and Ca^{2+} ions enter the cytoplasmic compartment through TRPV1 channels localized in the plasma membrane [4]. Functionally active TRPV1 channels are also present in the ER membrane ($TRPV1_{ER}$), depleting intracellular Ca^{2+} stores upon activation [5,6]. However, the sensitivity of $TRPV1_{ER}$ to exogenous activators is lower than that of the plasma membrane-embedded TRPV1 [7]. The channel can be activated by elevated temperature (>43 °C) [4], both acidic and basic pH [8], or by exo- and endovanilloids such as capsaicin (CAPS), resiniferatoxin (RTX) [4], N-arachidonoyl-dopamin [9] or anandamide [10]. On the contrary, TRPV1 is blocked with the channel blocker, Ruthenium Red (RuRed) [11] and with competitive antagonists such as capsazepine [12]. In the past, TRPV1 expression was assumed to be selective for pain-sensing sensory neurons [13]. However, TRPV1 expression was detected in various organs including brain, kidney, lung, testis, pancreas, spleen, liver, stomach, skin, muscle and in cell lines derived from those [14–16]. Interestingly, TRPV1 overstimulation leading to cytotoxicity was only reported for neurons suggesting that either I) expression levels of TRPV1 in non-neuronal tissues are low, II) neurons are particularly vulnerable or III) the physiological function of the TRPV1 channel is different in various organs [17]. One caveat of the above mentioned studies is that the authors did not consider that the samples used for the identification of TRPV1 might be “contaminated” with neuronal TRPV1-positive C and

* Corresponding author at: Unit of Anatomy, Department of Medicine, University of Fribourg, Route Albert-Gockel 1, CH-1700 Fribourg, Switzerland. Tel.: +41 26 300 85 08; fax: +41 26 300 97 33.
E-mail address: Beat.Schwaller@unifr.ch (B. Schwaller).

Aδ fibers that enmesh all internal organs. In addition, discordant results were obtained with two probably non-specific antibodies against TRPV1 resulting in different expression patterns, e.g. in the skin [18,19]. In line with the above concerns, Cre-recombinase expression driven by the TRPV1 promoter was mostly restricted to peripheral neurons in transgenic mice [20].

Depending on the concentration applied and the exposure time, TRPV1 agonists cause either desensitization [21] or selective degeneration of a distinct population of primary sensory neurons involved in the mediation of pain [22]. Systemic administration of CAPS results in the death of approximately 50% of sensory neurons in rat neonates [13] and in a loss of approximately 17% in adult rats [23]. RTX, an ultrapotent CAPS analogue, almost completely eliminates TRPV1-expressing afferent neurons in adult rats, when applied systemically [24]. Thus, selective ablation of pain-sensing neurons by administration of TRPV1 agonists may be effective in chronic pain treatment [25]; topical CAPS formulations have already been used for pain management [26]. The intrathecal administration of RTX went into a clinical trial to treat severe cancer-mediated pain [27]. However, the mechanisms by which TRPV1 agonists exert their cyto-/neuro-toxic effects are not fully understood.

Calretinin (CR) is a cytosolic Ca^{2+} buffer protein from the large family of EF-hand proteins, characterized by fast Ca^{2+}-binding kinetics [28] and may have additional functions, possibly as a Ca^{2+} sensor [29]. CR is expressed in specific populations of neurons in the central and peripheral nervous systems [30] and in certain cancer cells [31,32]. In neurons, CR was proposed to be implicated in neuroprotection. CR-expressing cortical neurons are selectively resistant to excitotoxicity *in vitro* [33] and ectopic CR expression delays the onset of cell death in glutamate-sensitive P19 cells [34] and protects N18-RE105 neuroblastoma-retina cells from glutamate-induced excitotoxicity [35]. In this study, we set out to investigate whether CR also has a protective effect against CAPS-induced, TRPV1-mediated "neurotoxicity." Beforehand we elaborated on the mechanisms of CAPS-induced cell death in an *in vitro* model system using TRPV1-expressing fibroblasts (NIH3T3). Activation of the TRPV1 channel led to entry of Ca^{2+} and mostly Na^{+}, the latter causing water influx and associated volume increase in TRPV1-expresing cells. The rapid volume increase caused a proportion of cells to lose plasma membrane integrity and to die by a necrotic, caspase-3/7-independent mechanism. Entry of Ca^{2+} via plasma membrane TRPV1 channels increased the effect on volume increase and cell death and the presence of CR attenuated the CAPS-mediated effects and consequently prevented/delayed cell death.

2. Materials and methods

2.1. Reagents

Thapsigargin, ionomycin (IONO), N-methyl-D-glucamine (NMDG) and rat nerve growth factor were purchased from Sigma Aldrich (St. Louis, MO, USA). Capsaicin (CAPS) and Ruthenium Red (RuRed) were purchased from Tocris Bioscience (Bristol, UK). Fluo-3-AM, FuraRed-AM, calcein-AM, CoroNa-Green-AM and pluronic acid were from Invitrogen (Carlsbad, CA, USA).

2.2. Cell cultures and plasmids

NIH3T3 cells were grown in RPMI 1640 medium (Invitrogen) supplemented with 10% fetal calf serum, 100 U/ml penicillin-streptomycin (PEN-STREP). TRPV1-expressing NIH3T3 cells were a kind gift from Dr. Zoltan Olah, Szeged, BRC. In those cells, the metallothionein promoter is used to drive the expression of full-length rat TRPV1 with a short 12 amino acid ε-tag [5]. This promoter is slightly leaky. Without any induction, it provides a stable, permanent expression of TRPV1 protein [5]. All cultures were maintained in a humidified atmosphere at 37 °C and 5% CO_2. For the generation of a NIH3T3 and TRPV1/NIH3T3 cell line stably expressing a fusion protein termed eGFP-CR consisting of the enhanced green fluorescent protein (eGFP) as the N-terminal part and full-length human calretinin as the C-terminal part, the retroviral expression vector pLVTHM (Addgene plasmid 12247 [36]) was used. The GFP cassette in pLVTHM was replaced with the eGFP-CR cDNA (B. Schwaller and J. Antonov, unpublished). Briefly, the eGFP-CR insert was synthesized by PCR using the primers *PmeI*-eGFP (5′-GTTTAAACCGCCACCATGGTGAGCAAGGGC-3′) and *SpeI*-CR (5′-ACTAGTTTACATGGGGGGCTCGCTGCA3′) using the plasmid pEGFP-CR as template. The PCR fragment was subcloned into pGEM-T-easy (Promega). pGEM-T-easy was digested with *Pme*I and *Spe*I and the PCR amplicon inserted into the unique sites of the pLVTHM to produce the final pLVTH-eGFP-CR. The CMV-mRFP-CR plasmid coding for the monomeric red fluorescent protein (mRFP) was produced by inserting the CR sequence into the pDsRed-Monomer-C1 plasmid (Clontech, Mountain View, CA). Briefly, *Hind*III and *Kpn*I restriction endonuclease sites were incorporated into the CR PCR fragment amplified from pRSV-CR [34] using the forward 5′-GAGAAAGCTTTAGCTGGCCCGCAG CAGC-3′ and reverse 5′-GAGAGGTACCTTACATGGGGGGCTCGCTGCA-3′ primers, respectively. After digesting the PCR fragment with these enzymes, the size-separated DNA insert was ligated in pDsRed-Monomer-C1 at the compatible *Hind*III and *Kpn*I sites. The mRFP-CR-expressing NIH3T3 cells were generated by transient transfection using the TransIT®-2020 transfection reagent (Mirus Bio, Madison, WI, USA) following the manufacturer's instructions. All plasmids were verified by DNA sequencing. Lentivirus was produced by the calcium phosphate transfection method using HEK293T cells and three plasmids: expression plasmid (pLVTHM-eGFP-CR), envelope plasmid pMD2G-VSVG (Addgene plasmid 12259) and packaging plasmid (pCMV-dR8.91), a kind gift from Prof. D. Trono (EPFL, Lausanne). Viral supernatants were collected after 48 h and 72 h, filtered, aliquoted and frozen at −80 °C [37]. After infection of NIH3T3, HeLa or TRPV1/NIH3T3 cells, clones showing high fluorescence intensity, i.e. high protein expression levels, were selected for further experiments.

2.3. Primary DRG cultures

DRG primary cultures were prepared from embryonic rats (E15). Embryos were removed from the uterus and placed in Petri dishes containing Krebs-Ringer buffer (in mM: 119 NaCl, 4.7 KCl, 2.5 $CaCl_2$, 1.2. $MgSO_4$, 1.2 KH_2PO_4, 25 $NaHCO_3$, 2 glucose; pH 7.4). The cords were dissected and DRGs were removed. The tissue was digested in 0.05% trypsin at 37 °C for 10 min and dissociated cell cultures were maintained in DMEM containing 5% horse serum and 100 ng/ml nerve growth factor to promote neuronal survival and differentiation. After 2 days *in vitro* (DIV2) primary DRG cultures were analyzed using confocal microscopy (Leica TCS SP5).

2.4. Cobalt histochemistry

CAPS-induced activation of plasmalemmal TRPV1 was assessed by cobalt uptake. Cells seeded on glass coverslips at approximately 50% confluence were washed with physiological salt solution (0.9% NaCl) and then incubated for 10 min in the same solution containing 5 mM $CoCl_2$ and one of the following substances: 1) no additive (control); 2) CAPS (5 μM); 3) IONO (5 μM); 4) CAPS (5 μM) and Ruthenium Red (20 μM). Cells were washed 3-times with physiological salt solution. Cobalt taken up by activated TRPV1 channels was precipitated by adding a 2.5% β-mercaptoethanol solution in physiological salt solution for 5 min. Cells were fixed in 4% paraformaldehyde solution and mounted. Pictures from the slides with cobalt precipitate were taken with a light microscope DM RBE (Leica, Wetzlar, Germany).

2.5. Calcium imaging

Cells grown on collagen-coated glass bottom 35 mm dishes (MatTek Corp., Ashland, MA) were loaded with the cell permeable acetoxymethyl (AM)-ester form of the indicator dyes. The following dyes were used: for Ca^{2+}, Fluo-3 (3 μM) and FuraRed (5 μM) (Invitrogen) diluted in culture medium for 1 h at 37 °C, for Na^{+}, CoroNa Green (10 μM) diluted in Krebs buffer for 30 min at 37 °C. Pluronic acid (0.01%) was added to facilitate dye uptake. The buffer solution (DPBS) used for Ca^{2+} imaging experiments contained (in mM): NaCl 138, Na_2HPO_4 8, $CaCl_2$ 2, $MgCl_2$ 0.5, KCl 2.7, KH_2PO_4 1.6, pH 7.4. In NMDG solutions, NaCl and Na_2HPO_4 were replaced with equimolar N-methyl-D-glucamine (NMDG). In low Ca^{2+} solution, $CaCl_2$ was replaced with equimolar NaCl. We used an inverted confocal microscope DMI6000 integrated to a Leica TCS-SP5 workstation or an inverted fluorescence microscope DMI6000B (Leica) to examine changes of either $[Ca^{2+}]_i$ or $[Na^{+}]_i$. For the ratiometric Ca^{2+} measurements, cells were simultaneously loaded with Fluo-3 and FuraRed. The 488-nm wavelength was used to illuminate the cells. At the confocal microscope, fluorescence emission was recorded at 505–550 nm (Fluo-3, CoroNa Green) and 665 to 685 nm (FuraRed). Fluo-3/FuraRed ratio images were calculated by dividing pixel values of Fluo-3 fluorescence intensity by pixel values of FuraRed fluorescence intensity. At the inverted fluorescence microscope the additional Leica filters were used: L5 for GFP, TX2 for FuraRed. Recordings were performed at room temperature (22 °C), since pharmacological properties of TRPV1 with respect to CAPS are not significantly different from the ones at 37 °C [17]. The drugs were added to the above-mentioned solutions either by pipette or an Octaflow system (ALA Scientific Instruments, Farmingdale, USA) and remained in the solution until the end of the experiments. Fluorescence images for either $[Ca^{2+}]_i$ or $[Na^{+}]_i$ measurements and transmitted images for monitoring cell volume changes were collected simultaneously. About 95–99% of the TRPV1/NIH3T3 cells and about 75–85% of eGFP-CR/TRPV1/NIH3T3 cells responded to CAPS. Only these cells were chosen for data analysis. Circular-shaped regions of interest (ROI) were placed inside the cytoplasmic area of cells. The fluorescence values were calculated after background subtraction (fluorescence intensity of regions without cells). Fluorescence intensity values were normalized in each experiment to the averaged basal value measured during the non-treated period. Bleaching correction was carried out, when the baseline was not stable. The LAS-AF (Leica) and Prism3 (GraphPad Software, Inc., San Diego, CA) software were used for data analysis.

2.6. Cell volume estimation

Cell volumes were measured using two methods: the image analysis [38] and fluorescence analysis [39] methods. The image analysis technique allows to following the changes, both in the cell morphology and $[Ca^{2+}]_i$. In this case the transmitted images were evaluated. Cell borders were traced on the monitor with the use of the mouse. The surface area of traced regions was determined by the image analysis software ImageJ. The relative cell volume changes were determined by the following relationship:

$$\frac{V(t)}{V(0)} = \sqrt{(S(t))^3}/\sqrt{(S(0))^3}$$

where $V(t)$ is the cell volume at time point t; $V(0)$ is the cell volume before treatment; $S(t)$ is the surface area at time point t; $S(0)$ is the surface area before treatment.

The fluorescence cell volume measurement is based on the dilution of the dye calcein. Calcein is a fluorescent dye that is not sensitive to the changes in either $[Ca^{2+}]_i$ or $[Na^{+}]_i$ at physiological pH. Cells were loaded with 2 μM calcein-AM in cell medium at 37 °C for 30 min. Excitation was performed at 488 nm, and the emitted fluorescence was measured at 517 nm. The relative cell volume changes were determined by the following equation:

$$\frac{V(t)}{V(0)} = F(0)/F(t)$$

considering that: $V(0)^*C(0) = V(t)^*C(t)$ and $C(0)/C(t) = F(0)/F(t)$, where $V(t)$ is the cell volume at time point t; $V(0)$ is the cell volume before treatment; $F(t)$ is the fluorescence intensity of calcein at time point t: $F(0)$ is fluorescence intensity of calcein before treatment; $C(t)$ is the calcein concentration at time point t, $C(0)$ is the calcein concentration before treatment. A comparison of two methods for measuring cell volume revealed no significant difference between the two.

2.7. Immunohistochemistry

Mice were anesthetized with pentobarbital (0.5 ml/kg i.p.; Eutha 77®; Essex Pharma GmbH, München) and then transcardially perfused with physiological salt solution followed by 4% paraformaldehyde (pH 7.4). The lumbal DRGs and TGs were quickly removed, postfixed with paraformaldehyde, cryoprotected in 30% sucrose, embedded in OCT compound (Ted Pella, Inc., Redding, CA), frozen, and sectioned on a Microm HM550 cryostat (Zeiss, Oberkochen, Germany). Sections of 10-μm thickness were cut and mounted on SuperFrost glass slides (Thermo Fisher Scientific, Waltham, MA). TG and DRG sections were circled with a water-resistant pen (DakoCytomation A/S, Glostrup, Denmark) and pre-treated with a blocking solution of 0.1% Triton X-100 and 1% donkey serum (Sigma-Aldrich) in PBS for 1 h. Then slides were co-incubated with a mix of rabbit anti-mouse TRPV1 antibody (1:1000, Genetex, San Antonio, USA) and goat anti-CR antibody CG1 (1:300, SWant, Bellinzona) in PBS overnight at 4 °C. After washing with PBS, sections were incubated with Cy3-conjugated donkey anti-rabbit IgG (1:500, Jackson, USA) and Alexa-488-conjugated donkey anti-goat IgG (1:2000, Jackson) for 2 h at 37 °C. Slides were counterstained with 10 μg/ml DAPI (Invitrogen) in Tris-buffered saline for 10 min, and mounted with Hydromount solution (National Diagnostics, Atlanta, GA). Stained slides were photographed using a confocal microscope DMI6000 integrated to a TCS-SP5 workstation (Leica).

2.8. Western blotting

Protein samples were isolated from either cell lysates, rat or mouse tissue. Freshly excised rat or mouse trigeminal ganglia (TG) or dorsal root ganglia (DRG) were frozen in liquid nitrogen and homogenized in extraction buffer (10 mM Tris, pH 7.4, 2 mM EDTA, 1 mM β-mercaptoethanol) containing a cocktail of different protease inhibitors (Roche, Mannheim, Germany). Extraction buffer was also added to the trypsinized cells and then the soluble proteins were extracted by ultrasonication for 3 × 20 s. The suspension was centrifuged (12,000g, 4 °C, 20 min). Protein concentration in the supernatant was determined with the Bradford protein assay (Bio-Rad, Hercules, CA). Protein (0.3 μg) from each cell culture sample, 10 μg protein from TG and DRG, as well as 200 ng of purified CR were loaded on SDS-polyacrylamide gels (10%). After separation, proteins were transferred onto nitrocellulose membranes. After blocking with 5% fat milk powder the nitrocellulose membrane was treated overnight with rabbit anti-CR primary antibody diluted at 1:10,000. Appropriate secondary antibodies linked to horseradish peroxidase (Sigma-Aldrich) were diluted at 1:10,000. For the detection, a chemiluminescent reagent Luminata Classico Substrate (EMD Millipore Corporation, Billerica, MA, USA) was used. Chemiluminescent and normal illumination digital images were recorded on a system from Cell Biosciences (Santa. Clara, CA, USA).

2.9. Membrane integrity measurements

Cells were seeded on 24-well plates at 50% confluence. Cells were incubated in one of the following solutions: 1) DPBS; 2) DPBS with CAPS (5 μM); 3) low Ca^{2+} solution with CAPS (10 μM) and EDTA (10 μM); 4) NMDG solution and CAPS (10 μM); 5) DPBS + CAPS (10 μM) + RuRed (10 μM). After 90 min, cells were incubated with 1 μM propidium iodide (necrotic cell marker) and 1 μM Hoechst33342 to label all nuclei for 30 min. Pictures were taken with a Leica DMI 6000B fluorescence microscope. Cells with red and blue nuclei were counted and the ratio red/blue was calculated.

2.10. Cytotoxicity and caspases-3/7 activity measurements.

The ApoTox-Glo™ Triplex assay (Promega, Madison, WI, USA) was used to measure the activity of dead cell proteases and caspase-3/7 enzymes. TRPV1/NIH3T3 cells were seeded in black and white 96-well plates (Thermo Scientific, Roskilde, Denmark) at a density of 10,000 cells/well. After 2 and 4 h of CAPS exposure, the reagents were added and cells incubated for 30 min. The luminescence and the fluorescent intensity (at 485 nm excitation and 535 nm emission) were monitored with a Victor X3 2030 Multilabel Reader (Perkin Elmer, Waltham, Massachusetts).

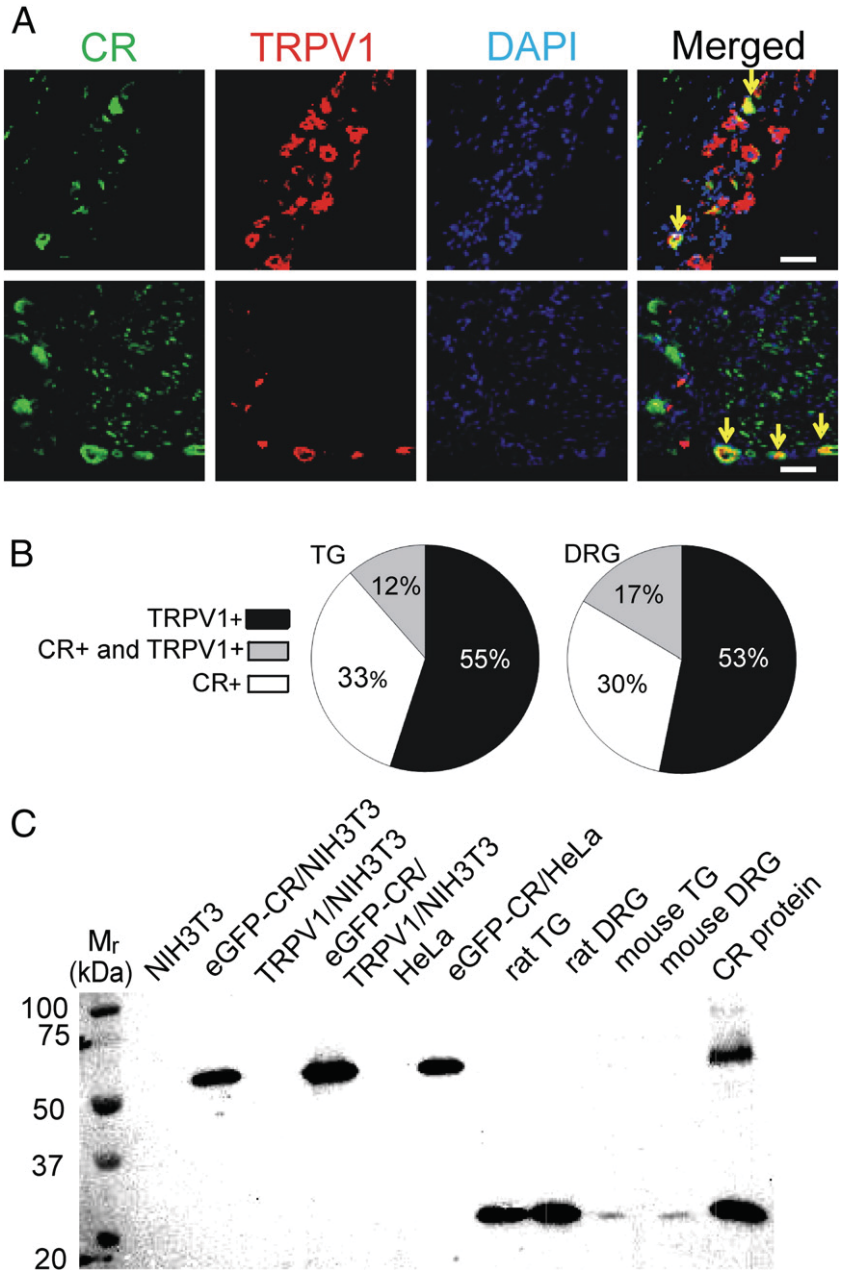

Fig. 1. Localization of TRPV1 and CR in DRG and TG neurons. A. Immunostaining shows TRPV1-positive (red) and CR-positive (green) neurons in the mouse DRG. To better identify individual neurons, nuclei were counterstained with DAPI (blue). Yellow arrows point to neurons expressing both TRPV1 and CR evidenced by the yellow color in the merged picture. Scale bar: 50 μm. B. Pie charts show the distribution of TRPV1- and CR-positive neurons in DRG (left) and TG (right). Approximately 7–8 non-consecutive slices were evaluated. C. Western blot analysis reveals the presence of CR (30 kDa) in rat and mouse TG and DRG tissue, and the fusion protein eGFP-CR (59 kDa) in samples from transfected NIH3T3 and HeLa cells. The upper band (60 kDa) in the sample of recombinant human CR used as a standard is a dimer resulting from long storage of purified CR as described before for other CaBPs [32].

3. Results and discussion

3.1. CR is expressed in a subset of TRPV1-positive DRG and TG neurons

We first investigated the expression of CR in peripheral nerve cells, in particular in dorsal root ganglion (DRG) and trigeminal (TG) neurons. In the mouse TG, CR-immunoreactive (CR-ir) neurons were of predominantly large and medium body size (~20% of the total neurons), while TRPV1-ir neurons were mainly small or medium-sized neurons (~35% of total neurons); double labeling was relatively rare and was observed in approximately 6% of neurons. About 27% of CR-ir neurons were also immunoreactive for TRPV1 and 18% of the TRPV1-ir neurons showed CR expression (Fig. 1A and B). The relative distribution of the 2 proteins in the DRG was similar; about 36% of CR-ir neurons co-expressed TRPV1 protein and 24% of the TRPV1-ir showed CR expression (Fig. 1A and B). Qualitatively similar immunohistochemistry results were also observed in rat TG and DRG neurons (data not shown). In mouse and also rat TG and DRG tissue, CR was expressed as evidenced by Western blot analysis (Fig. 1C). A protein band of approx. 30 kDa co-migrating with recombinant human CR was present in all samples. The weaker CR bands in mice tissue might have two reasons: I) excision of DRG and TG tissue in rat is more precise, thus less dilution by CR-negative surrounding tissue and II) CR expression levels in rat DRG and TG neurons might be higher than in mouse neurons.

The presence of CR in a sub-population of pain-sensing neurons has been reported before [40,41]; nociceptors-expressing neurons were identified by the presence of pain-related peptides, tachykinins. In the rat DRG, 7.2% of CR-ir neurons were tachykinin-ir and in the TG, a larger proportion of CR-ir cells (38.4%) showed tachykinin expression [41]. In this study, we identified the pain-sensitive neurons by TRPV1 immunohistochemistry. The distribution pattern of CR and TRPV1 in sensory ganglions was rather similar. This is not surprising, considering that TRPV1 strongly co-localizes with tachykinins, such as substance P [42] or with the tachykinin receptor NK1 [43].

3.2. Effects of CAPS on cultured DRG neurons

First, we investigated the effect of CAPS on increases in $[Ca^{2+}]_i$ and cell morphology in cultured embryonic rat DRG neurons. Upon CAPS administration, about 40% of neurons showed a marked increase in $[Ca^{2+}]_i$ characterized by the green and yellow color in Fig. 2A and $[Ca^{2+}]_i$ levels remained elevated until the end of the recording period (Fig. 2A and B). These cells correspond to the TRPV1-ir neurons as previously confirmed by others [4]. Most of the remaining neurons did not show any changes in $[Ca^{2+}]_i$, however some cells exhibited CAPS-independent oscillations of $[Ca^{2+}]_i$. The CAPS-responsive cells also showed morphological changes. Some neurons became appreciably swollen, retracted their axons and then "exploded," i.e. losing the membrane integrity (Fig. 2A). Along some neuronal processes, membrane blebs appeared suggesting that actin attachment sites between the plasma membrane and the underlying cytoskeleton may be weakened by CAPS treatment (Fig. 2A).

At least two types of membrane blebs occurring during biological processes including cell movement, viral infections, cell division and cell death have been described [44]. The first one called "apoptotic blebs" is seen during apoptosis, cell division or cell movement; blebs are small, short-lived (few minutes) and they can retract. In contrast, necrotic blebs are large and translucent; their size increases over long periods of time, they cannot retract [44], are independent of actomyosin contraction [45] and their growing is based on the influx of ions and water [39]. Although CAPS-induced blebs along DRG neuron processes were small, they did not retract and grew continuously during the observation period indicative of necrotic blebs. In rat DRG neurons, similar findings were reported before, e.g. after RTX

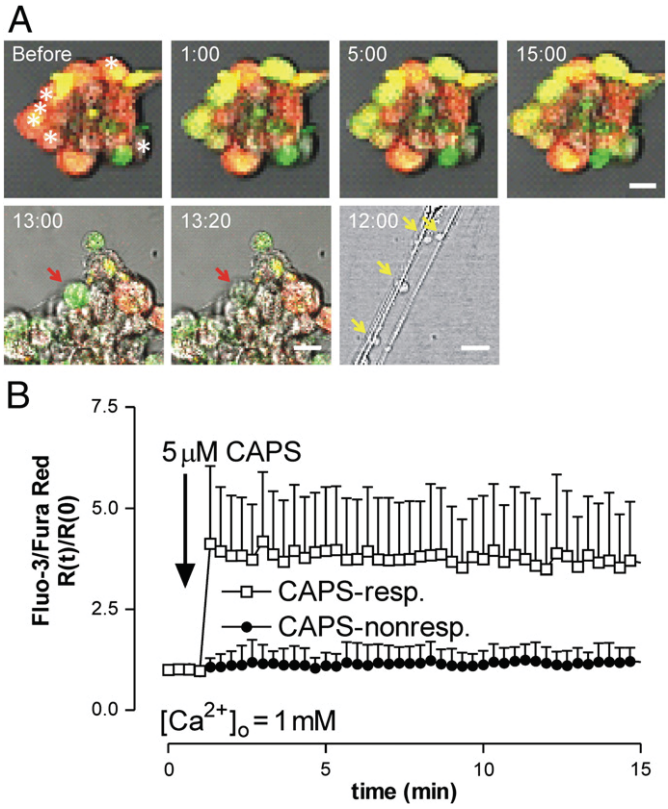

Fig. 2. TRPV1-mediated toxicity in cultured rat DRG neurons *in vitro*. A. Time-lapse microscopy shows primary DRG neurons loaded with the Ca^{2+} indicators Fluo-3/FuraRed. Cells with basal (low) $[Ca^{2+}]_i$ show orange/red color. After CAPS (5 µM) administration, approximately 40% of primary DRG neurons (examples marked with white asterisks) display an increase in $[Ca^{2+}]_i$ evidenced by yellow/green color (upper row). Scale bar: 25 µm. Two sequential images show DRG neurons after 10 µM CAPS exposure. The membrane integrity of the neuron marked with a red arrow was likely impaired and the cell was bursting/exploding (necrotic cell death, lower row—left side). Scale bar: 10 µm. Yellow arrows demonstrate membrane blebs along the axons (lower row—right side). Scale bar: 10 µm. B. Time course of changes in the Fluo-3/FuraRed ratio in DRG neurons. CAPS caused a rapid increase in $[Ca^{2+}]_i$ in CAPS-responsive cells. Data are mean ± standard deviation (S.D.) from 10 cells. The experiment was repeated three times.

administration, [46] and in mouse neocortical neurons upon NMDA-receptor (over)activation [47].

3.3. Effects of CAPS on TRPV1-expressing NIH3T3 cells

To get a better mechanistic insight into the processes leading to the observed CAPS-induced, likely TRPV1-mediated changes in DRG neurons, we used as a model NIH3T3 cells with or without TRPV1 expression, thus allowing to selectively investigate the role of TRPV1. While TRPV1/NIH3T3 cells exposed to CAPS (5 µM) showed a rapid increase in $[Ca^{2+}]_i$ that persisted during the recording period of 15 min, control NIH3T3 did not respond to CAPS application (Fig. 3A and B). After the rapid elevation of $[Ca^{2+}]_i$ within the first minute of CAPS application, $[Ca^{2+}]_i$ levels later on were more variable, but on average stayed around values reached shortly (<2 min) after CAPS application (Fig. 3B). Resulting from CAPS application, cell roundening and swelling, as well as the appearance of membrane blebs was evident selectively in TRPV1/NIH3T3 cells (Fig. 3A). Cell swelling was quantitatively analyzed: a constant increase in cell volume reaching approximately 200% after 10 min was observed (Fig. 3C). The morphology of NIH3T3 control cells was indistinguishable from untreated cells (data not shown). Thus, in all further experiments, NIH3T3 cells were used as a negative control, although a small CAPS-dependent increase of $[Ca^{2+}]_i$ in a subclone of NIH3T3 cells has been reported before [48]. In our hands NIH3T3 cells were

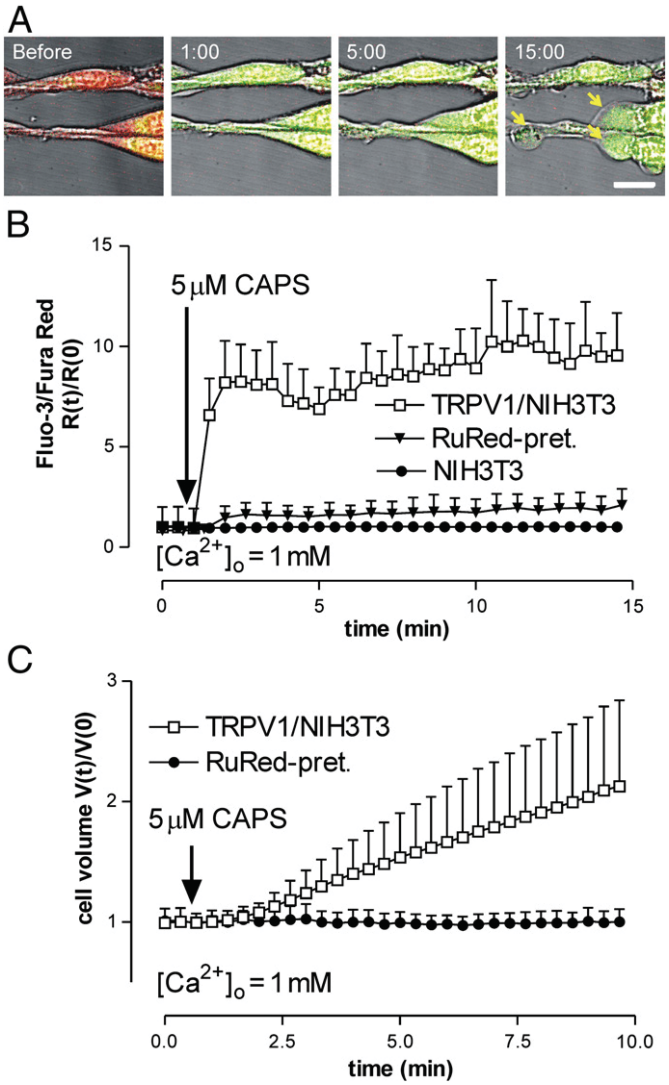

Fig. 3. TRPV1-mediated toxicity in TRPV1/NIH3T3 cells. A. Time-lapse microscopy images show TRPV1-expressing NIH3T3 cells loaded with intracellular Ca^{2+} indicators exposed to CAPS (5 μM). TRPV1/NIH3T3 cells show a rise in $[Ca^{2+}]_i$, (change from orange/red to yellow/green), swelling of the cell body, retraction of protrusions and membrane blebbing at 15 min (yellow arrows). Scale bar: 25 μm. B. Time course of changes in Fluo-3/FuraRed ratio signal in NIH3T3 cells with or without expression of TRPV1. CAPS causes an increase in $[Ca^{2+}]_i$ in TRPV1-expressing cells that is mostly prevented by pretreatment (pret.) of cells with RuRed, a blocker of plasmalemmal TRPV1. C. Cell volume increase caused by CAPS administration, which is prevented by RuRed. Data in B and C are mean ± S.D. from 10 cells. Diagrams are representative of 3 separate experiments showing similar results.

non-responsive to CAPS treatment. Blocking of the functional TRPV1 channels in the plasma membrane by the membrane-impermeant RuRed inhibited cell swelling (Fig. 3C) except in a very few cases and considerably decreased the CAPS-evoked increase in $[Ca^{2+}]_i$ (Fig. 3B). The remaining much smaller Ca^{2+} signal (Fig. 3B) was caused by the CAPS-mediated activation of $TRPV1_{ER}$, since the lipophilic properties of CAPS allows it to cross the plasma membrane and to act on $TRPV1_{ER}$. The $TRPV1_{ER}$-mediated elevation in $[Ca^{2+}]_i$ are rather small: from 50 nM to approx. 100 nM [49,50] at zero extracellular $[Ca^{2+}]_o$. Of importance the small elevation in $[Ca^{2+}]_i$ after CAPS application in the presence of RuRed did not cause the cells to swell, i.e. to increase their volume (Fig. 3C). As the TRPV1/NIH3T3 cells showed similar morphological and intracellular $[Ca^{2+}]_i$ changes in response to CAPS application compared with the cultured DRG primary neurons, we used TRPV1/NIH3T3 cells for further experiments aimed to delineate the CAPS-induced mechanisms leading to swelling and cell death.

In cortical neurons, bleb formation, more precisely an increase in the size of varicosities was suggested to be caused by NMDA receptor activation leading to accumulation of excess $[Ca^{2+}]_i$, which in turn causes activation of calpain, a Ca^{2+}-dependent protease [47]. However, no calpain activation was seen in DRG neurons treated with RTX, despite clear elevations in $[Ca^{2+}]_i$ [46]. A crucial role of Na^+ influx in bleb formation on inner hair cells appearing during the isolation process of the organ of Corti was shown [51] and in hepatocytes, cell swelling evoked by free-radical exposure was attenuated in cells, whose Na^+ pump was inhibited with ouabain [52]. Finally, blocking a non-identified non-selective cation channel by flufenamic acid, inhibiting stretch-activated cation channels by Gd^{3+} or replacement of extracellular Na^+ with NMDG was also effective against free-radical induced necrosis in hepatocytes [39]. Thus, in the next series of experiments we investigated the effect of Na^+ ions on CAPS-mediated cell morphology alterations.

3.4. Na^+ influx through the TRPV1 channel

The TRPV1 channel is a non-specific cation channel permeable for Ca^{2+} ions, but also for Na^+ ions [4]. Channel opening by CAPS causes an increase in $[Ca^{2+}]_i$ from 0.1 μM up to 0.5–1 μM [49] and an increase in $[Na^+]_i$ from 5 mM up to 40 mM [53]. Since Na^+ is the major extracellular osmolyte and $[Na^+]_i$ shows the largest absolute change in intracellular concentrations upon TRPV1 activation, we first investigated the involvement of Na^+ overload in membrane blebbing. Measuring $[Na^+]_i$ with the indicator CoroNa-Green showed a rapid increase in $[Na^+]_i$ in TRPV1/NIH3T3 cells immediately after CAPS administration (Fig. 4A); $[Na^+]_i$ remained elevated during the recording period of 15 min, similar to the increase in $[Ca^{2+}]_i$ shown in Fig. 2B. In the absence of extracellular Na^+, cell swelling was blocked, demonstrating the pivotal role of an increase in $[Na^+]_i$ in this process (Fig. 4B). The addition of Na^+ (73 mM) to the extracellular solution 15 min after CAPS application resulted in an increase in $[Na^+]_i$ (Fig. 4D), while $[Ca^{2+}]_i$ remained unchanged (Fig. 4C). The increase in $[Na^+]_i$ in the extracellular solution evoked morphological changes; mainly membrane bleb formation rather than cell swelling (Fig. 4B).

In a previous study it was concluded that increased $[Ca^{2+}]_i$ and not $[Na^+]_i$ was the main determinant for TRPV1-mediated cytotoxicity [54]. The conclusions were based on the fact that application of the TRPV1 antagonists capsazepine or RuRed several minutes after CAPS application decreased $[Ca^{2+}]_i$, but did not reverse the elevated $[Na^+]_i$ in experiments lasting for up to 5 min. When monitoring cell death in TRPV1-transfected HEK293 cells 12–15 h after continuous CAPS exposure, cells treated with RuRed showed less cell death evidenced by propidium iodide uptake. In our view, these results do not preclude a role for Na^+ ions. The decrease in $[Na^+]_i$ to basal levels might take much longer for CAPS-treated TRPV1-expressing HEK293 [54] or NIH3T3 cells (our study). We did not determine how long it would take for $[Na^+]_i$ to reach basal levels after CAPS removal in TRPV1/NIH3T3 cells. However, also in neurons recovery from increased $[Na^+]_i$ is rather slow, in parallel to the rather long periods required for the retraction of transient membrane blebs. In cortical neurons it takes 2 h to revert blebs after removal of the glutamate receptor agonist NMDA [47]. Also neuronal cell swelling caused by veratridine, an activator of a voltage-gated Na^+ channels persisted for 90 min after drug removal [38].

3.5. Increasing $[Ca^{2+}]_o$ promotes Na^+ influx through TRPV1 channel

In the next series of experiments, we investigated the role of $[Ca^{2+}]_o$ on the CAPS-mediated effects. In the absence of extracellular $[Ca^{2+}]_o$ cell swelling (volume increase) was much slower and also the magnitude was much smaller 10 min after CAPS application (Fig. 5A) in comparison to $[Ca^{2+}]_o$ of 1 mM depicted in Fig. 3C. The small increase in $[Ca^{2+}]_i$ resulting from $TRPV1_{ER}$-mediated ER Ca^{2+} release was of similar

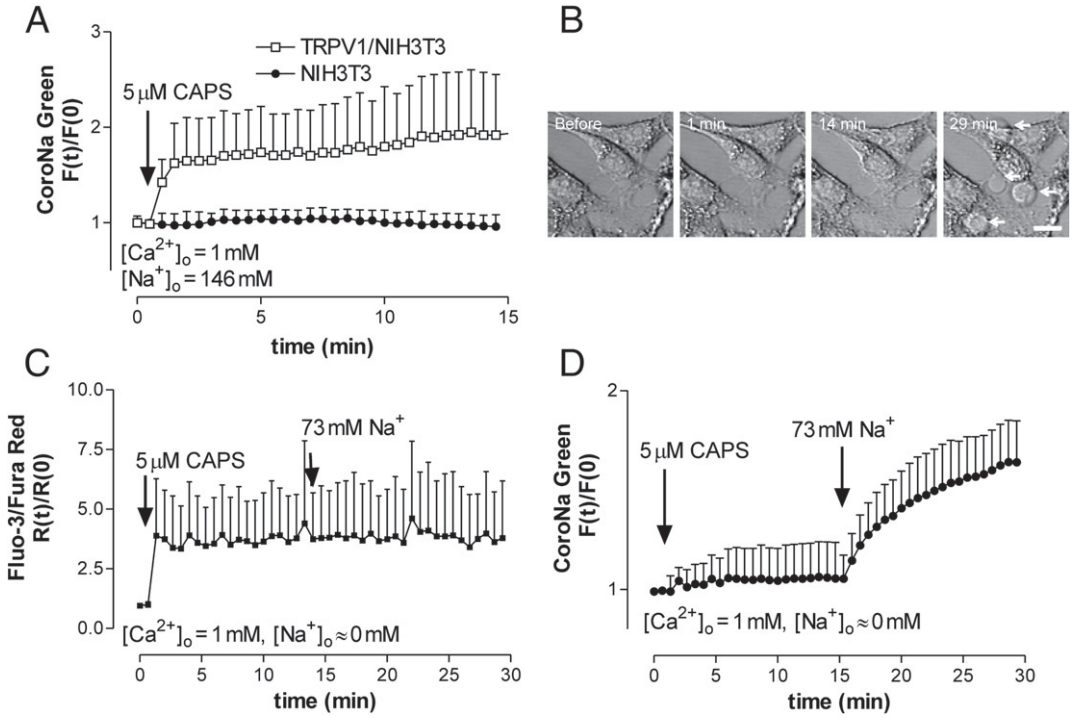

Fig. 4. Effect of Na^+ ions on cell swelling A. Application of CAPS (5 μM) causes a lasting increase in $[Na^+]_i$ in TRPV1-expressing cells. B. Images from time-lapse video reveal morphological changes of TRPV1/NIH3T3 cells. The low Na^+ media was replaced by one containing 73 mM Na^+ 14 min after CAPS administration. Membrane blebs (arrows on the image taken at 29 min) were evident only after increasing $[Na^+]_o$ and not during the first 15 min of CAPS application at low $[Na^+]_o$. C. An increase in $[Ca^{2+}]_i$ after CAPS administration occurred at low $[Na^+]_o$, and did not further increase when switching to 73 mM $[Na^+]_o$. D. Increase in $[Na^+]_i$ after increasing $[Na^+]_o$ to 73 mM in cells pretreated with CAPS at "zero" $[Na^+]_o$. All graphs depict results from 10 cells (mean ± S.D.). One representative experiment out of three is shown.

magnitude as observed after blocking of plasma membrane TRPV1 by RuRed (Fig. 3B). Increasing $[Ca^{2+}]_o$ to 0.5 mM resulted in a rapid increase in $[Ca^{2+}]_i$ (Fig. 5B) and concomitantly to an increase in cell volume (Fig. 5A). However, no membrane bleb formation was observed. Measuring the $[Na^+]_i$ increase upon TRPV1 activation revealed that $[Na^+]_i$ elevations were clearly slower in the absence of extracellular Ca^{2+} ions (Fig. 5C).

These results suggest that although Na^+ influx via TRPV1 channels is the main contributor to the cell volume increase, Ca^{2+} ions modulating the function of TRPV1 also participate in the cell swelling process. The increased Na^+ influx rate in the presence of extracellular Ca^{2+} is the likely result of an increased permeability for Na^+ across the TRPV1 channels, and not by an increased driving force. As our experiments started at resting potential, the initial Na^+ driving force should be the same, independent of $[Ca^{2+}]_o$. Thus, the presence of extracellular Ca^{2+} ions might evoke its modulating effect on Na^+ influx in at least two ways: I) modifying the TRPV1 pore size to make it more suitable for Na^+ transport or II) increasing the open-state probability of TRPV1 channels.

A role for increased $[Ca^{2+}]_i$ in membrane bleb formation was previously provided in experiments using the TRPV1 agonists CAPS and the more potent RTX. In DRG neurons, the latter caused a six-fold higher membrane loss (bleb formation) compared to CAPS; this increase was due to longer lasting elevations in $[Ca^{2+}]_i$ in the presence of RTX, while the maximum increase in $[Ca^{2+}]_i$ evoked by short RTX treatment was not different from the one induced by CAPS [6]. Thus, the authors concluded that "the prolonged elevations in $[Ca^{2+}]_i$ may potentiate RTXs toxicity." Ionic currents through TRPV1 channels are different at higher $[Ca^{2+}]_o$: the reduction in the ratio of Ca^{2+} and Na^+ ion permeability (P_{Ca}/P_{Na}) is the consequence of prolonged activation of TRPV1 channels, which causes activation-evoked modifications in the TRPV1 pore structure [55]. At low $[Ca^{2+}]_o$, TRPV1 channels show a time-dependent increase in the P_{Ca}/P_{Na} ratio. In other words, high $[Ca^{2+}]_o$ renders TRPV1 channels more permeable to Na^+ ions than to Ca^{2+} ions and these results are consistent with our data.

3.6. Increase in $[Ca^{2+}]_i$ activates/sensitizes TRPV1 channels

To test the hypothesis that increased $[Ca^{2+}]_i$ sensitizes/activates TRPV1 channels, we increased $[Ca^{2+}]_i$ by either IONO or thapsigargin. In control NIH3T3 cells IONO caused a transient peak of $[Ca^{2+}]_i$ lasting for approx. 2 min; however $[Ca^{2+}]_i$ levels did not completely recover to pre-IONO conditions (Figs. 6B and 7A). IONO makes the plasma membrane leaky to Ca^{2+} ions and additionally promotes Ca^{2+} release from internal stores [56]. Thus, the first transient peak observed immediately after IONO addition is caused by ER Ca^{2+} release, while the later phase is governed by IONO-mediated, IONO concentration-dependent plasma membrane Ca^{2+} influx [57]. The decrease in $[Ca^{2+}]_i$ was the likely result from increased Ca^{2+} extrusion and/or organellar Ca^{2+} uptake, because no changes in membrane integrity evidenced by propidium iodide exclusion were observed (data not shown).

In TRPV1-expressing NIH3T3 we could distinguish two cell subpopulations based on their response to IONO. In the first population (p1), IONO caused a single Ca^{2+} peak similar to that seen in control NIH3T3 cells (Fig. 6B). In p1 cells CAPS administration 4 min after IONO treatment evoked a second, robust $[Ca^{2+}]_i$ increase (Fig. 6B). In the second population (p2), $[Ca^{2+}]_i$ remained elevated after IONO treatment and the sequential CAPS administration resulted in an additional, but rather minor increase in $[Ca^{2+}]_i$ (Fig. 6B). The proportion of the p2 subpopulation ranged from 24% to 55% in individual experiments. A likely explanation for the different effects seen in p1 and p2 cells is possibly linked to different TRPV1 expression levels and/or IONO sensitivity. We hypothesize that only in p2 cells IONO-induced elevations in $[Ca^{2+}]_i$ were sufficient for robust TRPV1 activation and thus addition of CAPS had a minor additional effect. Upon IONO treatment membrane

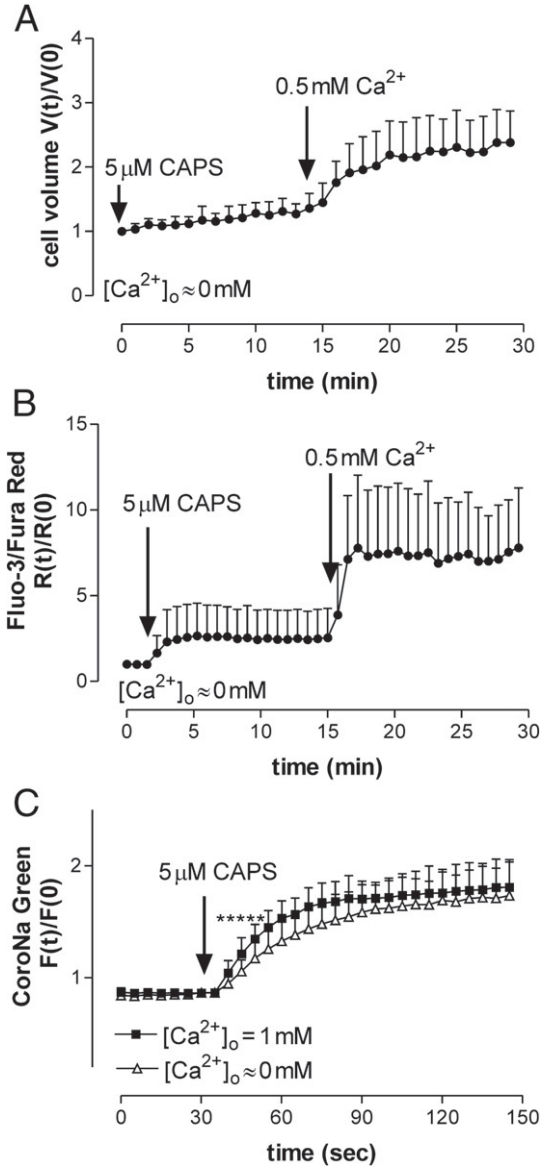

Fig. 5. Effect of Ca^{2+} ions on cell swelling A. Low $[Ca^{2+}]_o$ strongly attenuated and slowed down cell swelling. Relative cell volumes ($n = 10$ cells) were evaluated by the video imaging method. Media containing Ca^{2+} (0.5 mM final concentration) was administered 15 min after CAPS exposure. One representative experiment out of three is shown. B. In the absence of $[Ca^{2+}]_o$, the increase in $[Ca^{2+}]_i$ after CAPS application was rather small, in comparison to the increase in $[Ca^{2+}]_i$ observed after rising $[Ca^{2+}]_o$ to 0.5 mM. Data in B. and C. are mean ± S.D. from 10 cells. One representative experiment out of three is shown. C. The rate in rise of $[Na^+]_i$ was slower in "zero" $[Ca^{2+}]_o$, but plateau levels of $[Na^+]_i$ reached after approx. 90 s were similar. The traces on the graph show average values from seven individual experiments. Asterisks indicate significant differences ($p < 0.05$).

blebs appeared only in TRPV1/NIH3T3-p2 cells, while control NIH3T3 and p1 cells did not show any morphological changes again indicating that high $[Ca^{2+}]_i$ is required and sufficient to activate TRPV1 channels that led to an increase in cell volume and bleb formation (Fig. 6A).

The above results were further validated in control NIH3T3 and TRPV1/NIH3T3cells by cobalt accumulation experiments. Treatment with CAPS (5 μM) or IONO (5 μM) resulted in a robust or minor cobalt accumulation in TRPV1/NIH3T3 cells, respectively (Fig. 6C). The CAPS-induced precipitate could be prevented by RuRed (not shown). In the absence of CAPS or IONO, but incubation with the cobalt solution, TRPV1/NIH3T3 cells showed no brownish cobalt precipitate (Fig. 6C). In control NIH3T3 cells, the addition of CAPS and IONO did not result in cobalt accumulation (Fig. 6C).

A similar effect has been previously reported in DRG neurons: the CAPS-mediated increase in $[Ca^{2+}]_i$ was about twofold larger when CAPS was added shortly after addition of thapsigargin, [6] and also Ca^{2+} mobilization by carbachol led to TRPV1 activation [58]. We hypothesize that TRPV1 can sense elevated $[Ca^{2+}]_i$ by an intracellular Ca^{2+} sensor domain or in cooperation with a Ca^{2+} sensor protein. Other members of the TRP superfamily are candidates for the store-operated Ca^{2+} channels that are activated by elevated $[Ca^{2+}]_i$ due to ER depletion [59]. In the case of TRPC1, the Ca^{2+} sensor protein STIM1 transmits the elevated $[Ca^{2+}]_i$ signal to the channel [60].

3.7. Calretinin modulates Ca^{2+} signals in NIH3T3 and TRPV1/NIH3T3 cells

Since CR is expressed in a sub-population of TRPV1-ir neurons, the role of CR in CAPS-mediated cell morphology changes was analyzed in the NIH3T3 model system using control NIH3T3 cells, TRPV1/NIH3T3 cells and additionally in HeLa cells, all of which showed no endogenous CR expression evidenced by Western blot analysis (Fig. 1C). In order to directly assess relative CR expression levels we used constructs coding for fusion proteins consisting of either eGFP or mRFP as the N-terminal part followed by full-length CR as the C-terminal part. Stably eGFP-CR expressing clones were established by lentivirus infection of the above cell lines, followed by cloning by limiting dilution. Testing of CR protein expression in selected clones revealed the clones to contain considerable amounts of CR (Fig. 1C). Sufficiently high CR expression levels were considered as a requirement in order to detect changes in CR-expressing and non-expressing clones, since also the Ca^{2+} indicator dyes act as Ca^{2+} buffers. Cells with or without CR expression were mixed, plated on coverslips and analyzed with respect to Ca^{2+} signaling. Recordings from the green channel allowed to distinguish CR-expressing from non-expressing cells, while simultaneously recording $[Ca^{2+}]_i$ with FuraRed detected on the red channel. There was no interference between the two channels. The eGFP-CR and control cells were undistinguishable on the red channel under basal conditions. Moreover, comparing the IONO-evoked $[Ca^{2+}]_i$ trace in NIH3T3 cells with or without eGFP (without the CR part) showed that eGFP alone does not modify Ca^{2+} signals (data not shown).

CR decreased the maximal amplitude of $[Ca^{2+}]_i$ as previously observed in other CR-transfected cells subjected to glutamate-induced elevations in $[Ca^{2+}]_i$ [34]. However, the kinetics of the recovery phase ($[Ca^{2+}]_i$ decay) was clearly slowed down, both in NIH3T3 (Fig. 7A) and HeLa cells (not shown) after IONO administration. The effect of CR on CAPS-induced elevations in $[Ca^{2+}]_i$ are shown in Fig. 7B. First, we observed that the initial rise in $[Ca^{2+}]_i$ within the first 30 s after CAPS administration was slower in CR-expressing cells. Moreover, the maximal value during the plateau phase remained always lower in eGFP-CR/TRPV1/NIH3T3 cells than in TRPV1/NIH3T3 cells without CR expression (Fig. 7B). In parallel, the increase in volume was clearly smaller in the CR-expressing cells (Fig. 7C) and also bleb formation was less pronounced (data not shown). Along the same line, also the CAPS-induced increase in $[Na^+]_i$ in cells expressing mRFP-CR was significantly lower just shortly after CAPS application, at later time points (>1 min after CAPS treatment) these difference disappeared (Fig. 7D). Nonetheless, the CR-provoked decrease in cell volume persisted for at least 15 min (Fig. 7C). This indicates that the relative small difference in maximal $[Ca^{2+}]_i$ after CAPS application in the presence of CR translates into a relative large effect with respect to cell swelling and associated volume increase, despite minor effects on $[Na^+]_i$. Our results suggest that CR evokes its effect by its Ca^{2+}-buffering function, limiting the maximal amplitude of CAPS-mediated increase in $[Ca^{2+}]_i$. However, we cannot exclude the possibility that CR might also modulate TRPV1 activity via an interaction with other proteins affecting TRPV1 channel function or directly with the TRPV1 channel. We have summarized the molecular mechanisms underlying the cell swelling caused by prolonged TRPV1 activation in the scheme shown in Fig. 8.

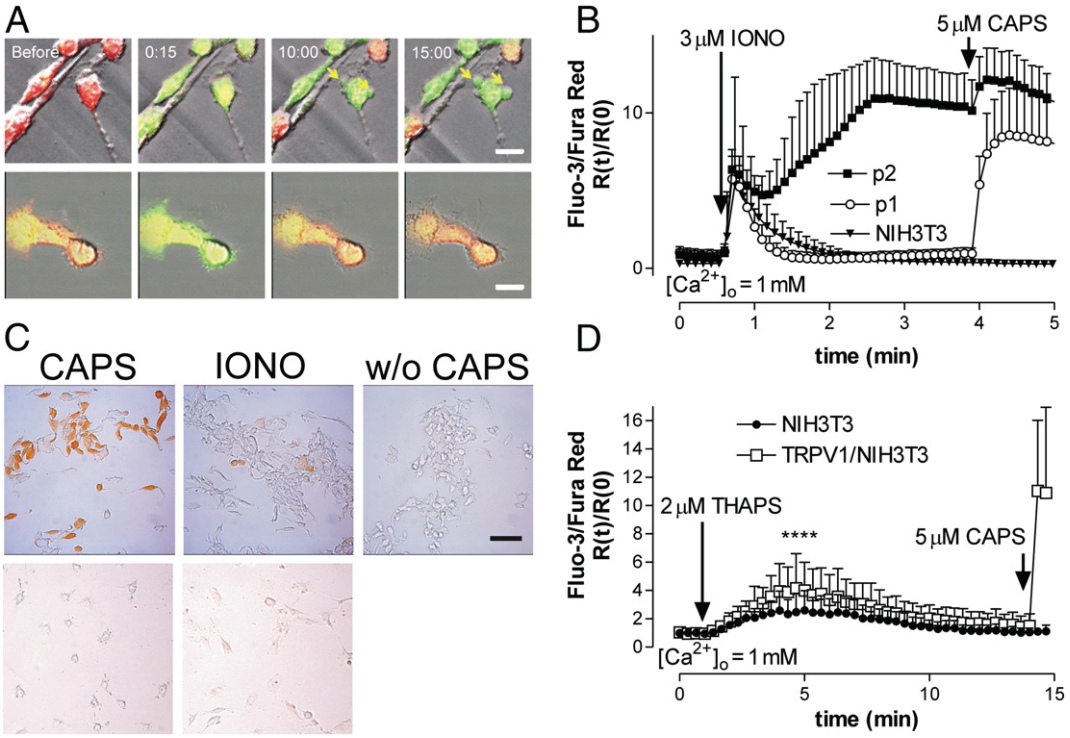

Fig. 6. Elevated $[Ca^{2+}]_i$ sensitizes/activates TRPV1 receptors. A. Time-lapse confocal images show the effect of IONO on NIH3T3 cells with (upper row) or without TRPV1 expression (lower row). Several TRPV1/NIH3T3 cells show a rise in $[Ca^{2+}]_i$, cell swelling and membrane blebs (yellow arrows) after addition of IONO (3 μM). Scale bars: 25 μm. B. IONO application leads to a transient increase in $[Ca^{2+}]_i$ in control NIH3T3 cells ($n = 10$ cells) and in a subpopulation (p1) of TRPV1-expressing cells ($n = 10$ cells). The application of CAPS (5 μM) 4 min later induces a strong $[Ca^{2+}]_i$ increase in p1, but not control cells. In the second sub-population p2, $[Ca^{2+}]_i$ remains elevated after IONO treatment and addition of CAPS has a much smaller effect resulting in only a small additional increase in $[Ca^{2+}]_i$. One representative experiment out of three is shown. C. Cobalt histochemistry reveals the function of plasmalemmal TRPV1 after CAPS or IONO treatment in TRPV1/NIH3T3 (upper row) and in control NIH3T3 cells (lower row). Scale bar: 50 μm. D. TRPV1-expressing NIH3T3 cells show increased $[Ca^{2+}]_i$ upon thapsigargin (2 μM) treatment, possibly caused by partial TRPV1 activation. Data are mean ± S.D. from 10 cells and the graph is representative for 3 separate experiments showing similar results.

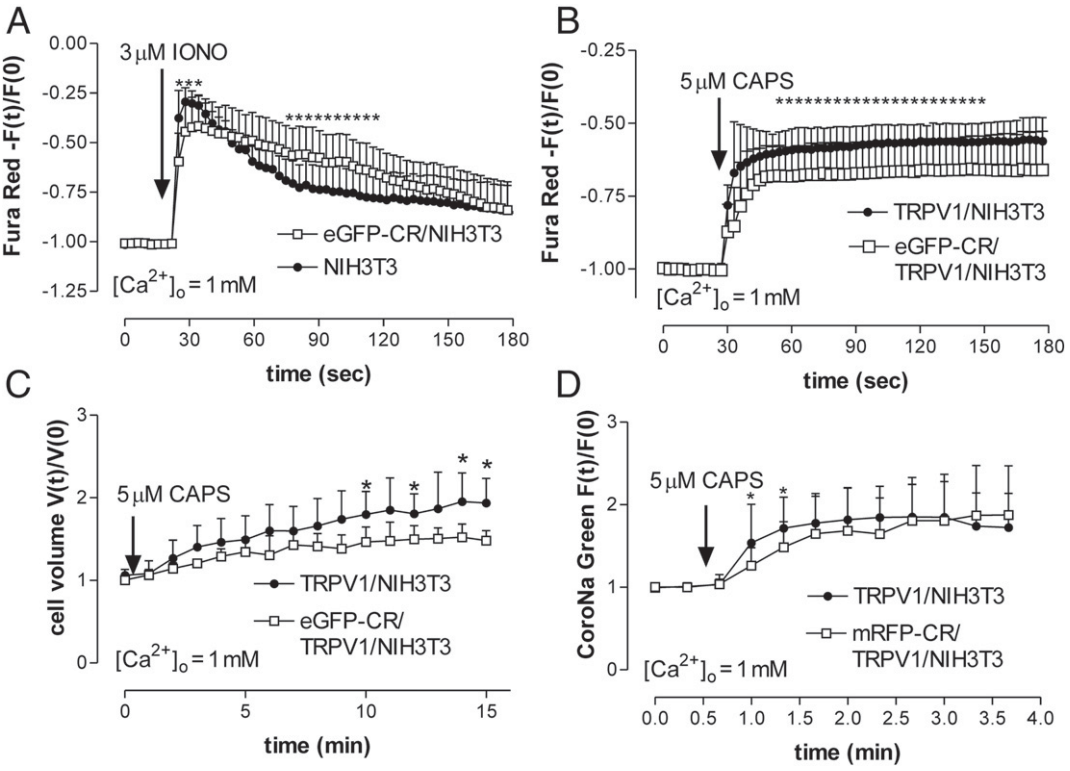

Fig. 7. The effect of CR on NIH3T3 cells with or without TRPV1 expression. A. The presence of eGFP-CR (CR) modulates IONO-induced $[Ca^{2+}]_i$ transients: CR decreases the peak amplitude in $[Ca^{2+}]_i$, but slows down recovery of $[Ca^{2+}]_i$. B. The CAPS-induced rise in $[Ca^{2+}]_i$ is slower in NIH3T3/TRPV1 cells and the maximal amplitude is lower in CR expressing cells. C. CR expression diminishes the CAPS-induced volume increase. D. In cells expressing mRFP-CR, the CAPS-induced $[Na^{+}]_i$ elevation in NIH3T3/TRPV1 cells is slowed down. In all cases, data are mean ± S.D. from 10 cells. Graphs are representative of 3 separate experiments showing similar results. Asterisks indicate significant differences ($p < 0.05$).

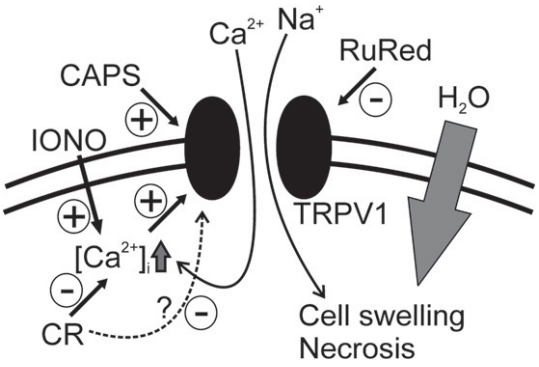

Fig. 8. Proposed model for the molecular mechanism of cell swelling induced by prolonged TRPV1 activation. The cell swelling is the consequence of Na^+ influx via activated TRPV1 channels and concomitant H_2O transport. The presence of extracellular Ca^{2+} ions might evoke its positive modulating effect on Na^+ influx in at least two ways: i) modifying the TRPV1 pore size to make it more suitable for Na^+ transport or ii) increasing the open-state probability of TRPV1 channels by elevation of $[Ca^{2+}]_i$. Besides the well-known TRPV1 agonist CAPS, an elevation of $[Ca^{2+}]_i$ by the Ca^{2+} ionophore ionomycin (IONO) or other factors can also activate/sensitize TRPV1 channels. This effect can be blocked by the addition of the membrane impermeant Ruthenium Red (RuRed). The presence of CR in the cytosol blunts peak $[Ca^{2+}]_i$ and eliminates/decreases the TRPV1 activation mediated by an increase in $[Ca^{2+}]_i$. Whether the effect of CR is solely the result of CR's Ca^{2+}-buffering properties or indirectly mediated by binding to a TRPV1-modulating protein or directly to TRPV1 channels remains to be determined. Positive modulation of TRPV1 is marked by "+," negative modulation/inhibition by "−." Solid arrows show experimentally proven regulation and the dashed arrow indicates hypothetical modulation of TRPV1 (e.g. by CR).

A role of Ca^{2+}-binding proteins in conferring resistance to Ca^{2+} overload has been demonstrated in several systems. Calretinin-expressing neurons were relatively spared after exposure to either NMDA, glutamate or Ca^{2+} ionophore [33]. The expression of calretinin also protected N18-RE 105 neuroblastoma-retina hybrid N18 cells against excitotoxic cell death [35]. Calretinin delayed the onset of cell death after excitotoxic stimulation in transfected P19 cells [34]. In Huntington's disease, where the excitotoxic effect of glutamatergic striatal inputs originating from the thalamus and cerebral cortex might play a role in disease progression, the calretinin-positive interneurons were preferentially spared [61].

3.8. Prominent Na^+ influx contributes to CAPS-induced TRPV1-mediated cell death

To demonstrate that the fast cell-killing effects of high doses (10 μM) of CAPS is based on its ability to induce efficient and prominent Na^+ and water influx with which TRPV1-expressing NIH3T3 cells cannot cope, we measured the cell membrane integrity under different conditions. In TRPV1/NIH3T3 cells CAPS-treated under control conditions, approximately 50% cells stained positive for propidium iodide (PI) (Fig. 9A). A significant decrease in the proportion of impaired (PI-positive) cells was encountered in the presence of RuRed or the absence of either Ca^{2+} or Na^+ ions in the extracellular medium. Moreover, cells expressing calretinin were also protected to the same degree as cells treated with the TRPV1 inhibitor RuRed or cells subjected to CAPS treatment in the absence of extracellular Ca^{2+} or Na^+ ions. NIH3T3 cells without TRPV1 expression were not sensitive to CAPS-induced cytotoxicity (Fig. 9A).

Finally, we investigated the mechanism leading to CAPS-mediated cytotoxicity by simultaneously analyzing the activity of dead cell proteases, markers for necrotic cell death and caspase-3/7, markers for apoptosis. Based on the previous experiments, we hypothesized a CAPS-induced mostly necrosis-like process. Two and four hours of CAPS treatment resulted in concentration-dependent increase in markers of necrosis, while no evidence for caspase-3/7 activation, a marker for the intrinsic apoptosis pathway, was observed (Fig. 9B).

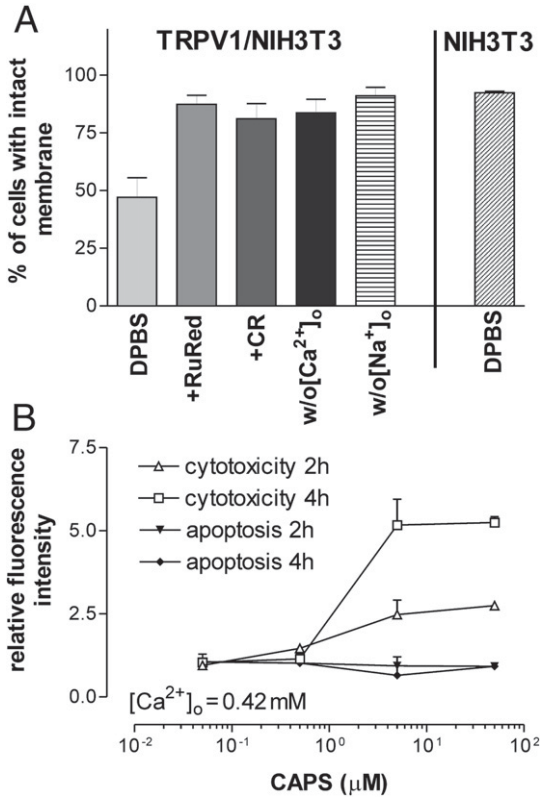

Fig. 9. Cell swelling impairs membrane integrity and leads to necrotic cell death. A. In control NIH3T3 cells, the addition of CAPS (10 μM) in DPBS solution does not significantly decrease the proportion of intact (propidium iodide-negative) cells, while this ratio is decreased to less than 50% in TRPV1/NIH3T3 cells 2 h after CAPS application. All of the following "treatments" prevent/diminish loss of membrane integrity: blocking of plasmalemmal TRPV1 with RuRed, expression of CR, CAPS treatment in "zero" $[Ca^{2+}]_o$ or "zero" $[Na^+]_o$. Three independent experiments were evaluated. Data are mean ± SD. B. CAPS treatment of TRPV1/NIH3T3 cells for 2 and 4 h results in a dose-dependent increase in cytotoxicity (necrosis) with no caspase-3/7 (apoptosis) activation. The experiment was repeated two times.

Acute cytotoxicity was seen only at higher CAPS concentrations, 5 and 50 μM.

The cellular and molecular mechanisms underlying the CAPS-induced neural loss are still unresolved. Evidences for CAPS-induced neuronal cell death by apoptosis with caspase activation have been reported [62,63], while some studies state that it is an apoptosis-like, but caspase-independent process [64,65]. Yet other studies doubt the process to be apoptosis at all [5,46]. It is very likely that several mechanisms might play a role in TRPV1-mediated toxicity also depending on the cell type and moreover on the experimental protocol.

An essential role for Ca^{2+} ions in the extracellular milieu for CAPS-induced cytotoxicity has been reported before [54] and was also confirmed in our study. Moreover, we demonstrated the pivotal role of Na^+ influx; our data show that CAPS treatment for 2–4 h causes a loss of membrane integrity typical for necrosis loss due to prominent Na^+ and water influx (Fig. 8). We suggest that this mainly occurred in those cells, where the TRPV1 surface density is high. This might then be followed by an apoptotic process, in which the continuously elevated $[Ca^{2+}]_i$ and possibly the resulting mitochondrial Ca^{2+} overload might trigger the apoptotic events as shown before [66]. When CAPS is applied at very high, millimolar concentrations, it can cause TRPV1-independent cell death [67]. Under these conditions CAPS replacing quinone in the mitochondrial respiratory chain inhibits energy production that finally leads to apoptosis. However, this was certainly not the case in our study, where in most experiments 5 μM CAPS was used.

4. Outlook

Considering that CR and TRPV1 co-expressing neurons are mainly medium size Aδ-type neurons, which are involved in fast-pain transmission, we may speculate that these neurons are much more resistant to Ca^{2+} and Na^{+} overload induced by repetitive activation of TRPV1 than the small mainly unmyelinated C-neurons, which are associated with chronic, dull pain.

The membrane bleb formation of C-fibers could explain the reversible reduction in intra-epidermal nerve fibers observed after 8% CAPS patch application [26]. The significant volume increase in sensory axons may result in severing/fragmentation or retraction of axons. This phenomenon we also observed *in vitro* on DRG axons and on the long protrusions of fibroblast cells. Comparing the effect of RTX and CAPS in different experiments [68], it was reported that although RTX binds 100,000-fold more effectively to TRPV1 than CAPS [69], the pungency test showed only a difference by a factor of 10 [70]. We may hypothesize that the RTX-evoked pain sensation and pain transmission is "reduced," by the fragmentation/severing of sensory axons due to the more pronounced membrane loss [46].

The similarities between the TRPV1-mediated neurotoxicity and the glutamate-receptor-mediated excitotoxicity are conspicuous. In both cases, ligand-gated channels form a pore for Ca^{2+} and Na^{+} ions. The permeability of TRPV1 to Ca^{2+} and Na^{+} ($P_{Ca}/P_{Na} = 9.6$) [4] is similar to values reported for NMDA glutamate receptors ($P_{Ca}/P_{Na} = 10.6$) [71]. The glutamate receptor activation by NDMA also causes membrane bleb formation in cortical neurons [47] and Na^{+} ions have already been proposed to be involved in neuronal cell death caused by glutamate receptor agonists [72,73]. Loss of pain-sensing neurons by TRPV1-mediated overstimulation is usually not a life-threatening situation, but loss of other neuron populations by excitotoxicity, e.g. motor neurons or cortical neurons, can cause severe conditions [74]. Because cell volume regulation is a critical step in both processes, a better understanding of the mechanisms of bleb formation might lead to identifying the steps involved in the development of excito-/neurotoxicity-related diseases.

Acknowledgments

The authors wish to thank Zoltan Olah for providing of stable TRPV1-expressing NIH3T3 cell line. The work was supported by an SNF grant to B.S. (no. 130680).

References

[1] A.E. Dubin, A. Patapoutian, Nociceptors: the sensors of the pain pathway, J. Clin. Invest. 120 (2010) 3760–3772.
[2] Y. Lee, C.H. Lee, U. Oh, Painful channels in sensory neurons, Mol. Cells 20 (2005) 315–324.
[3] M. Tominaga, T. Tominaga, Structure and function of TRPV1, Pflugers Arch. 451 (2005) 143–150.
[4] M.J. Caterina, M.A. Schumacher, M. Tominaga, T.A. Rosen, J.D. Levine, D. Julius, The capsaicin receptor: a heat-activated ion channel in the pain pathway, Nature 389 (1997) 816–824.
[5] Z. Olah, T. Szabo, L. Karai, C. Hough, R.D. Fields, R.M. Caudle, P.M. Blumberg, M.J. Iadarola, Ligand-induced dynamic membrane changes and cell deletion conferred by vanilloid receptor 1, J. Biol. Chem. 276 (2001) 11021–11030.
[6] L.J. Karai, J.T. Russell, M.J. Iadarola, Z. Olah, Vanilloid receptor 1 regulates multiple calcium compartments and contributes to Ca2+−induced Ca2+ release in sensory neurons, J. Biol. Chem. 279 (2004) 16377–16387.
[7] S. Gallego-Sandin, A. Rodriguez-Garcia, M.T. Alonso, J. Garcia-Sancho, The endoplasmic reticulum of dorsal root ganglion neurons contains functional TRPV1 channels, J. Biol. Chem. 284 (2009) 32591–32601.
[8] A. Dhaka, V. Uzzell, A.E. Dubin, J. Mathur, M. Petrus, M. Bandell, A. Patapoutian, TRPV1 is activated by both acidic and basic pH, J. Neurosci. 29 (2009) 153–158.
[9] D.R. Sagar, P.A. Smith, P.J. Millns, D. Smart, D.A. Kendall, V. Chapman, TRPV1 and CB(1) receptor-mediated effects of the endovanilloid/endocannabinoid N-arachidonoyl-dopamine on primary afferent fibre and spinal cord neuronal responses in the rat, Eur. J. Neurosci. 20 (2004) 175–184.
[10] V. Di Marzo, T. Bisogno, L. De Petrocellis, Anandamide: some like it hot, Trends Pharmacol. Sci. 22 (2001) 346–349.
[11] A. Dray, C.A. Forbes, G.M. Burgess, Ruthenium red blocks the capsaicin-induced increase in intracellular calcium and activation of membrane currents in sensory neurones as well as the activation of peripheral nociceptors in vitro, Neurosci. Lett. 110 (1990) 52–59.
[12] C.S. Walpole, S. Bevan, G. Bovermann, J.J. Boelsterli, R. Breckenridge, J.W. Davies, G.A. Hughes, I. James, L. Oberer, J. Winter, R. Wrigglesworth, The discovery of capsazepine, the first competitive antagonist of the sensory neuron excitants capsaicin and resiniferatoxin, J. Med. Chem. 37 (1994) 1942–1954.
[13] P. Holzer, Capsaicin: cellular targets, mechanisms of action, and selectivity for thin sensory neurons, Pharmacol. Rev. 43 (1991) 143–201.
[14] B. Veronesi, M. Oortgiesen, The TRPV1 receptor: target of toxicants and therapeutics, Toxicol. Sci. 89 (2006) 1–3.
[15] M.H. Vos, T.R. Neelands, H.A. McDonald, W. Choi, P.E. Kroeger, P.S. Puttfarcken, C.R. Faltynek, R.B. Moreland, P. Han, TRPV1b overexpression negatively regulates TRPV1 responsiveness to capsaicin, heat and low pH in HEK293 cells, J. Neurochem. 99 (2006) 1088–1102.
[16] M.J. Gunthorpe, A. Szallasi, Peripheral TRPV1 receptors as targets for drug development: new molecules and mechanisms, Curr. Pharm. Des. 14 (2008) 32–41.
[17] L. Pecze, K. Szabo, M. Szell, K. Josvay, K. Kaszas, E. Kusz, T. Letoha, J. Prorok, I. Koncz, A. Toth, L. Kemeny, C. Vizler, Z. Olah, Human keratinocytes are vanilloid resistant, PLoS One 3 (2008) e3419.
[18] N. Boulais, L. Misery, The epidermis: a sensory tissue, Eur. J. Dermatol. 18 (2008) 119–127.
[19] P. Facer, M.A. Casula, G.D. Smith, C.D. Benham, I.P. Chessell, C. Bountra, M. Sinisi, R. Birch, P. Anand, Differential expression of the capsaicin receptor TRPV1 and related novel receptors TRPV3, TRPV4 and TRPM8 in normal human tissues and changes in traumatic and diabetic neuropathy, BMC Neurol. 7 (2007) 11.
[20] S.K. Mishra, S.M. Tisel, P. Orestes, S.K. Bhangoo, M.A. Hoon, TRPV1-lineage neurons are required for thermal sensation, EMBO J. 30 (2011) 582–593.
[21] S. Mandadi, M. Numazaki, M. Tominaga, M.B. Bhat, P.J. Armati, B.D. Roufogalis, Activation of protein kinase C reverses capsaicin-induced calcium-dependent desensitization of TRPV1 ion channels, Cell Calcium 35 (2004) 471–478.
[22] G. Jancso, E. Kiraly, A. Jancso-Gabor, Pharmacologically induced selective degeneration of chemosensitive primary sensory neurones, Nature 270 (1977) 741–743.
[23] G. Jancso, E. Kiraly, F. Joo, G. Such, A. Nagy, Selective degeneration by capsaicin of a subpopulation of primary sensory neurons in the adult rat, Neurosci. Lett. 59 (1985) 209–214.
[24] S.R. Chen, H.L. Pan, Loss of TRPV1-expressing sensory neurons reduces spinal mu opioid receptors but paradoxically potentiates opioid analgesia, J. Neurophysiol. 95 (2006) 3086–3096.
[25] M.A. Schumacher, Transient receptor potential channels in pain and inflammation: therapeutic opportunities, Pain Pract. 10 (2010) 185–200.
[26] P. Anand, K. Bley, Topical capsaicin for pain management: therapeutic potential and mechanisms of action of the new high-concentration capsaicin 8% patch, Br. J. Anaesth. 107 (2011) 490–502.
[27] M.J. Iadarola, A.J. Mannes, The vanilloid agonist resiniferatoxin for interventional-based pain control, Curr. Top. Med. Chem. 11 (2011) 2171–2179.
[28] B. Schwaller, I. Durussel, D. Jermann, B. Herrmann, J.A. Cox, Comparison of the Ca2+-binding properties of human recombinant calretinin-22k and calretinin, J. Biol. Chem. 272 (1997) 29663–29671.
[29] B. Schwaller, The continuing disappearance of "pure" Ca2+ buffers, Cell. Mol. Life Sci. 66 (2009) 275–300.
[30] F. Barinka, R. Druga, Calretinin expression in the mammalian neocortex: a review, Physiol. Res. 59 (2010) 665–677.
[31] V. Gotzos, P. Vogt, M.R. Celio, The calcium binding protein calretinin is a selective marker for malignant pleural mesotheliomas of the epithelial type, Pathol. Res. Pract. 192 (1996) 137–147.
[32] J.C. Gander, M. Bustos-Castillo, D. Stuber, W. Hunziker, M. Celio, B. Schwaller, The calcium-binding protein calretinin-22k, an alternative splicing product of the calretinin gene is expressed in several colon adeno carcinoma cell lines, Cell Calcium 20 (1996) 63–72.
[33] W. Lukas, K.A. Jones, Cortical neurons containing calretinin are selectively resistant to calcium overload and excitotoxicity in vitro, Neuroscience 61 (1994) 307–316.
[34] C. D'Orlando, B. Fellay, B. Schwaller, V. Salicio, A. Bloc, V. Gotzos, M.R. Celio, Calretinin and calbindin D-28k delay the onset of cell death after excitotoxic stimulation in transfected P19 cells, Brain Res. 909 (2001) 145–158.
[35] C. D'Orlando, M.R. Celio, B. Schwaller, Calretinin and calbindin D-28k, but not parvalbumin protect against glutamate-induced delayed excitotoxicity in transfected N18-RE 105 neuroblastoma-retina hybrid cells, Brain Res. 945 (2002) 181–190.
[36] M. Wiznerowicz, D. Trono, Conditional suppression of cellular genes: lentivirus vector-mediated drug-inducible RNA interference, J. Virol. 77 (2003) 8957–8961.
[37] R.H. Kutner, X.Y. Zhang, J. Reiser, Production, concentration and titration of pseudotyped HIV-1-based lentiviral vectors, Nat. Protoc. 4 (2009) 495–505.
[38] K.B. Churchwell, S.H. Wright, F. Emma, P.A. Rosenberg, K. Strange, NMDA receptor activation inhibits neuronal volume regulation after swelling induced by veratridine-stimulated Na+ influx in rat cortical cultures, J. Neurosci. 16 (1996) 7447–7457.
[39] L.F. Barros, A. Stutzin, A. Calixto, M. Catalan, J. Castro, C. Hetz, T. Hermosilla, Nonselective cation channels as effectors of free radical-induced rat liver cell necrosis, Hepatology 33 (2001) 114–122.
[40] V.A. Movsesyan, A.G. Yakovlev, E.A. Dabaghyan, B.A. Stoica, A.I. Faden, Ceramide induces neuronal apoptosis through the caspase-9/caspase-3 pathway, Biochem. Biophys. Res. Commun. 299 (2002) 201–207.

[41] H. Ichikawa, S. Mitani, H. Hijiya, T. Nakago, D.M. Jacobowitz, T. Sugimoto, Calretinin-immunoreactivity in trigeminal neurons innervating the nasal mucosa of the rat, Brain Res. 629 (1993) 231–238.
[42] B. Banerjee, B.K. Medda, Z. Lazarova, N. Bansal, R. Shaker, J.N. Sengupta, Effect of reflux-induced inflammation on transient receptor potential vanilloid one (TRPV1) expression in primary sensory neurons innervating the oesophagus of rats, Neurogastroenterol. Motil. 19 (2007) 681–691.
[43] H. Zhang, C.L. Cang, Y. Kawasaki, L.L. Liang, Y.Q. Zhang, R.R. Ji, Z.Q. Zhao, Neurokinin-1 receptor enhances TRPV1 activity in primary sensory neurons via PKCepsilon: a novel pathway for heat hyperalgesia, J. Neurosci. 27 (2007) 12067–12077.
[44] M. Bovellan, M. Fritzsche, C. Stevens, G. Charras, Death-associated protein kinase (DAPK) and signal transduction: blebbing in programmed cell death, FEBS J. 277 (2010) 58–65.
[45] L.F. Barros, T. Kanaseki, R. Sabirov, S. Morishima, J. Castro, C.X. Bittner, E. Maeno, Y. Ando-Akatsuka, Y. Okada, Apoptotic and necrotic blebs in epithelial cells display similar neck diameters but different kinase dependency, Cell Death Differ. 10 (2003) 687–697.
[46] R.M. Caudle, L. Karai, N. Mena, B.Y. Cooper, A.J. Mannes, F.M. Perez, M.J. Iadarola, Z. Olah, Resiniferatoxin-induced loss of plasma membrane in vanilloid receptor expressing cells, Neurotoxicology 24 (2003) 895–908.
[47] B.T. Faddis, M.J. Hasbani, M.P. Goldberg, Calpain activation contributes to dendritic remodeling after brief excitotoxic injury in vitro, J. Neurosci. 17 (1997) 951–959.
[48] L.L. Zhang, D. Yan Liu, L.Q. Ma, Z.D. Luo, T.B. Cao, J. Zhong, Z.C. Yan, L.J. Wang, Z.G. Zhao, S.J. Zhu, M. Schrader, F. Thilo, Z.M. Zhu, M. Tepel, Activation of transient receptor potential vanilloid type-1 channel prevents adipogenesis and obesity, Circ. Res. 100 (2007) 1063–1070.
[49] B.J. Wisnoskey, W.G. Sinkins, W.P. Schilling, Activation of vanilloid receptor type I in the endoplasmic reticulum fails to activate store-operated Ca2+ entry, Biochem. J. 372 (2003) 517–528.
[50] J. Castro, E.C. Aromataris, G.Y. Rychkov, G.J. Barritt, A small component of the endoplasmic reticulum is required for store-operated Ca2+ channel activation in liver cells: evidence from studies using TRPV1 and taurodeoxycholic acid, Biochem. J. 418 (2009) 553–566.
[51] X. Shi, P.G. Gillespie, A.L. Nuttall, Na+ influx triggers bleb formation on inner hair cells, Am. J. Physiol. Cell Physiol. 288 (2005) C1332–C1341.
[52] R. Carini, R. Autelli, G. Bellomo, E. Albano, Alterations of cell volume regulation in the development of hepatocyte necrosis, Exp. Cell Res. 248 (1999) 280–293.
[53] S. Onizuka, T. Yonaha, R. Tamura, N. Hosokawa, Y. Kawasaki, M. Kashiwada, T. Shirasaka, I. Tsuneyoshi, Capsaicin indirectly suppresses voltage-gated Na+ currents through TRPV1 in rat dorsal root ganglion neurons, Anesth. Analg. 112 (2011) 703–709.
[54] E.R. Grant, A.E. Dubin, S.P. Zhang, R.A. Zivin, Z. Zhong, Simultaneous intracellular calcium and sodium flux imaging in human vanilloid receptor 1 (VR1)-transfected human embryonic kidney cells: a method to resolve ionic dependence of VR1-mediated cell death, J. Pharmacol. Exp. Ther. 300 (2002) 9–17.
[55] M.K. Chung, A.D. Guler, M.J. Caterina, TRPV1 shows dynamic ionic selectivity during agonist stimulation, Nat. Neurosci. 11 (2008) 555–564.
[56] C. Liu, T.E. Hermann, Characterization of ionomycin as a calcium ionophore, J. Biol. Chem. 253 (1978) 5892–5894.
[57] J.P. Kao, J.M. Alderton, R.Y. Tsien, R.A. Steinhardt, Active involvement of Ca2+ in mitotic progression of Swiss 3T3 fibroblasts, J. Cell Biol. 111 (1990) 183–196.
[58] M. van der Stelt, M. Trevisani, V. Vellani, L. De Petrocellis, A. Schiano Moriello, B. Campi, P. McNaughton, P. Geppetti, V. Di Marzo, Anandamide acts as an intracellular messenger amplifying Ca2+ influx via TRPV1 channels, EMBO J. 24 (2005) 3026–3037.
[59] C. Montell, The TRP superfamily of cation channels, Sci. STKE 2005 (2005) re3.
[60] J.P. Yuan, W. Zeng, G.N. Huang, P.F. Worley, S. Muallem, STIM1 heteromultimerizes TRPC channels to determine their function as store-operated channels, Nat. Cell Biol. 9 (2007) 636–645.
[61] M. Massouh, M.J. Wallman, E. Pourcher, A. Parent, The fate of the large striatal interneurons expressing calretinin in Huntington's disease, Neurosci. Res. 62 (2008) 216–224.
[62] H.W. Jin, H. Ichikawa, M. Fujita, T. Yamaai, K. Mukae, K. Nomura, T. Sugimoto, Involvement of caspase cascade in capsaicin-induced apoptosis of dorsal root ganglion neurons, Brain Res. 1056 (2005) 139–144.
[63] C.Y. Shin, J. Shin, B.M. Kim, M.H. Wang, J.H. Jang, Y.J. Surh, U. Oh, Essential role of mitochondrial permeability transition in vanilloid receptor 1-dependent cell death of sensory neurons, Mol. Cell. Neurosci. 24 (2003) 57–68.
[64] V.A. Movsesyan, B.A. Stoica, A.G. Yakovlev, S.M. Knoblach, P.M.t. Lea, I. Cernak, R. Vink, A.I. Faden, Anandamide-induced cell death in primary neuronal cultures: role of calpain and caspase pathways, Cell Death Differ. 11 (2004) 1121–1132.
[65] J.W. Davies, A.H. Hainsworth, C.J. Guerin, D.G. Lambert, Pharmacology of capsaicin-, anandamide-, and N-arachidonoyl-dopamine-evoked cell death in a homogeneous transient receptor potential vanilloid subtype 1 receptor population, Br. J. Anaesth. 104 (2010) 596–602.
[66] C. Giorgi, F. Baldassari, A. Bononi, M. Bonora, E. De Marchi, S. Marchi, S. Missiroli, S. Patergnani, A. Rimessi, J.M. Suski, M.R. Wieckowski, P. Pinton, Mitochondrial Ca(2+) and apoptosis, Cell Calcium 52 (2012) 36–43.
[67] T. Yagi, Inhibition by capsaicin of NADH-quinone oxidoreductases is correlated with the presence of energy-coupling site 1 in various organisms, Arch. Biochem. Biophys. 281 (1990) 305–311.
[68] A. Szallasi, P.M. Blumberg, Vanilloid (Capsaicin) receptors and mechanisms, Pharmacol. Rev. 51 (1999) 159–212.
[69] G. Acs, J. Lee, V.E. Marquez, P.M. Blumberg, Distinct structure-activity relations for stimulation of 45Ca uptake and for high affinity binding in cultured rat dorsal root ganglion neurons and dorsal root ganglion membranes, Brain Res. Mol. Brain Res. 35 (1996) 173–182.
[70] A. Szallasi, P.M. Blumberg, Resiniferatoxin, a phorbol-related diterpene, acts as an ultrapotent analog of capsaicin, the irritant constituent in red pepper, Neuroscience 30 (1989) 515–520.
[71] M.L. Mayer, G.L. Westbrook, Permeation and block of N-methyl-D-aspartic acid receptor channels by divalent cations in mouse cultured central neurones, J. Physiol. 394 (1987) 501–527.
[72] L.A. Raymond, A. Moshaver, W.G. Tingley, R.L. Huganir, Glutamate receptor ion channel properties predict vulnerability to cytotoxicity in a transfected nonneuronal cell line, Mol. Cell. Neurosci. 7 (1996) 102–115.
[73] T. Itoh, A. Itoh, K. Horiuchi, D. Pleasure, AMPA receptor-mediated excitotoxicity in human NT2-N neurons results from loss of intracellular Ca2+ homeostasis following marked elevation of intracellular Na+, J. Neurochem. 71 (1998) 112–124.
[74] B. Meldrum, J. Garthwaite, Excitatory amino acid neurotoxicity and neurodegenerative disease, Trends Pharmacol. Sci. 11 (1990) 379–387.